GRID SETUPS AND NUMERICAL SIMULATIONS OF A LOW BOOM CONCEPT AT OFF-DESIGN FLIGHT CONDITIONS

J. Kirz, German Aerospace Center (DLR), Institute of Aerodynamics and Flow Technology, Lilienthalplatz 7, 38108 Braunschweig, Germany

Abstract

The accurate prediction of the sonic boom along all parts of the mission trajectory is essential for the development and certification of a future low boom supersonic commercial aircraft. In this paper, the C25D low-boom concept geometry from the Second AIAA Sonic Boom Prediction Workshop is used to conduct numerical simulations at off-design flight conditions with the DLR TAU code. The flight altitude and flight Mach number are varied to simulate a mission trajectory while the lift is kept constant. The focus of this paper is the evaluation of a core grid setup with a non-circular cross section and the assessment of the applicability of the grid deformation and the Chimera technique for the variation of angle of attack while the farfield grid remains aligned to the Mach cone. It is shown that both techniques are viable and that differences in the pressure signatures between both techniques are negligible. Using the grid deformation technique resulted in lower grid node numbers and thus lower computational cost. In addition, the sensitivities of varying flight conditions on the pressure fields are evaluated. It is shown that the pressure signatures are strongly affected by varying flight conditions. While the shape of the front part of the pressure signatures stays constant for all flight conditions and only the magnitude changes, the impact on the aft part of the signature is large. The shocks and expansions are adversely interacting if only Mach number or the altitude are changed. Especially, the magnitudes of the main expansions are increasing. The lowest peak interactions for the on-track pressure signature can be found for accelerating while climbing.

1. INTRODUCTION

After 27 years in service, the retirement of Concorde in 2003 ended the era of commercial supersonic civil flight. In the last years, an increasing demand for faster air travel can be observed, especially for small-sized business jet aircraft. Additionally, market studies showed that there is a rising market for supersonic air travel [1, 2]. A major barrier for the operation of supersonic aircraft is the sonic boom. According to current regulations like the FAR 91.817, the operation of civil supersonic aircraft is prohibited over land in most countries unless it will avoid a sonic boom to reach the surface. As a result, the mitigation of the sonic boom is essential for the development of a future supersonic aircraft with the certification to fly supersonically over land.

Concepts for supersonic civil aircraft can be divided into two categories. The aim of the first category is minimizing the sonic boom signature as well as the demonstration and certification of the low boom technology for supersonic overland flight. Typical cruise Mach numbers for this group are around and below 1.6 [3, 4]. The second category does not intend to achieve low boom characteristics and considers already existing supersonic technologies. Thus, supersonic overland flight for these aircraft will be prohibited over land, which requires deviations from great-circle routes [5]. Cruise Mach numbers for these concepts can be higher than for low boom concepts and range up to Mach 2.2 [6, 7].

The shape of the ground pressure signature of high boom aircraft like Concorde or fighter jets is a N-wave, while low boom signatures are less peaky. The reduction of the sonic boom is usually achieved by modifying the shape of the aircraft in such a way that shocks and expansions from different geometrical features interact and decrease in strength. It is assumed today that the reduction of the sonic boom of a small supersonic aircraft by modifying the shape is feasible to a point where it appears acceptable by the general population [8]. For this reason, research at German Aerospace Center (DLR) Institute of Aerodynamics and Flow Technology (AS) focuses on the low boom – low drag design of supersonic aircraft.

Recent research showed that numerical methods are suitable for the accurate prediction of the sonic boom signature of a particular configuration [9] and to optimize supersonic configurations with respect to a lower sonic boom [3, 10]. The general approach is to use computational fluid dynamics (CFD) for the near field simulation, extract pressure signatures at three to five body lengths distance from the vehicle and use these pressure signatures as input for the ground propagation code. After the ground propagation a loudness calculation algorithm is applied. It is part of current research which loudness measurement algorithm offers the best representation of the perceived noise by human ear.

The American Institute of Aeronautics and Astronautics (AIAA) Sonic Boom Prediction Workshop (SBPW) was established to assess the state-of-the-art of predicting sonic boom signatures with numerical methods. The first AIAA SBPW was held in January 2014. DLR did not actively participate in the first SBPW, but used the available data to develop techniques for the numerical near-field simulation of the sonic boom with the tools used at DLR [11]. The second SBPW was held in January 2017. DLR participated in the near-field part of the workshop [12] along with 10 other international participant groups from

research and industry [9]. The progress made between SBPW1 and SBPW2 for the prediction of near-field pressure signatures is quite significant [9].

While previous studies focus on simulations at as-designed cruise flight conditions, not much effort was put into simulations at off-design flight conditions. Deviations from the designed cruise flight conditions are common in the mission trajectory of a supersonic aircraft and have to be considered in the design process of a low boom aircraft. The mission trajectory of a supersonic aircraft usually features a segment of supersonic acceleration at constant altitude [5] or a fuel-optimized segment of acceleration during a slight descent [13]. For the operation of a civil supersonic aircraft over land this raises the question if the requirements on the low sonic boom characteristics can also be ensured at these flight conditions or how the flight trajectory has to be modified to achieve the best low boom characteristics on the ground.

For this reason, the objective of this study is to investigate the impact of supersonic off-design flight conditions on the near-field pressure signatures of a low boom concept to gain an understanding of the interaction of the shocks and expansions at different flight conditions.
Varying the flight conditions directly affects the lift, so the angle of attack has to be adjusted in order to keep the lift equal to the weight of the aircraft. The distinctive feature of numerical low boom simulations is the Mach cone aligned farfield, as shown in Chapter 3. As a result, the angle of attack cannot be adjusted by simply rotating the farfield as it is done in many subsonic cases. This requires special techniques for the rotation of the geometry. For this reason, the focus of this paper will be the application and comparison of the Chimera technique and grid deformation technique for the variation of the angle of attack.

2. NASA C25D LOW BOOM GEOMETRY

The second SBPW provided geometries with different complexities for the near-field CFD simulations. The most complex geometry of the workshop is the NASA C25D [4], which is used for this study. It is a full configuration with a cruciform tail and a flow-through nacelle (C25F). The C25D is optimized for a low on-track sonic boom signature on the ground [10]. Figure 1 shows the C25D geometry. The design has a body length of 32.92m and is optimized for a cruise condition of Mach 1.6 at an altitude of 15,760m.

FIG 1. Geometry of the NASA C25D case with flow-through nacelle provided by the second AIAA Sonic Boom Prediction Workshop

3. GRID SETUPS

The grid generation process plays an important role for the quality of the results of a numerical simulation. Grids used for the simulation of the sonic boom are different to many other applications. Since the pressure signatures are extracted at several body lengths, the flow solution has to be accurate sufficiently far from the geometry so that near-field interference is prevented. The commercial grid generation software CENTAUR by CentaurSoft [15] is used for the grid generation. The grids used for this study are inviscid grids with a symmetry plane. A best practice for grid generation based on [14] was developed by using the cases of the first and second AIAA Sonic Boom Prediction Workshops and has already been compared to other grid setups provided by the Sonic Boom Prediction Workshops [10, 11].

For this approach the volume grid can be divided into two parts, as shown in Figure 2:

- The unstructured core grid (brown part)
- The Mach-cone aligned hexahedral collar grid (grey part)

If only the sonic boom is of interest, the required surface grid resolution is relatively low, but the discretization and quality of the collar grid is of great importance, which is explained in chapters 3.2 and 3.3.

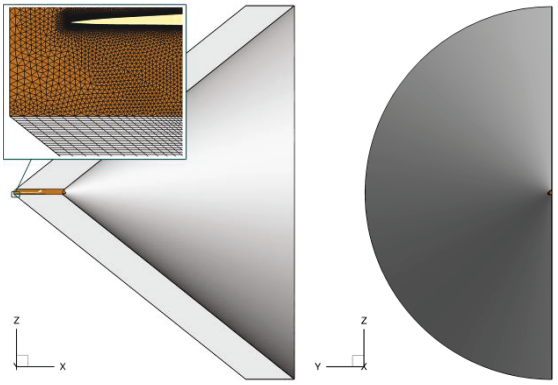

FIG 2. General grid setup for numerical simulations of the sonic boom

3.1. Grid Concepts for the Variation of the Angle of Attack

As pointed out earlier, the different flight conditions require changing the angle of attack dynamically during the simulations. One possible approach for changing the angle of attack is the generation of a new grid for each angle of attack. This approach has major disadvantages. Firstly, the effort for setting up the grid and the computational cost for the grid generation both are high. Since the angle of attack for the cases is not known in advance and has to be found iteratively, this process would take too long to be viable. Secondly, this approach does not guarantee an identical surface and near field grid for all cases which will lead to spurious effects.

These disadvantages can be prevented by using either of two advanced techniques implemented in the DLR TAU code. The first technique is the grid deformation technique in combination with modular grid generation. The modular grid generation approach is used to ensure an identical surface and near field grid when the farfield geometry is exchanged for different Mach angles, while the grid deformation allows changing the angle of attack for

different simulations at the same Mach number without having to create new grids. The grid deformation is performed using a radial basis function (RBF) approach [17].

The second approach is the Chimera overset grid technique [16]. For the Chimera technique two grids have to be generated. Firstly, the farfield grid and secondly the Chimera block with the C25D geometry, which has its own farfield. This ensures that the near-field grid is identical for all simulations. Only the farfield grid has to be generated for different Mach angles. The Chimera technique is applied in combination with an automatic Chimera hole cutting algorithm.

3.2. Surface and Core Grid

The surface grid has a general resolution of 433 points in streamwise direction. Sources are used to refine the grid at the nose as well as the leading and trailing edges of the wing, horizontal tail plane (HTP), vertical tail plane (VTP) and nacelle.

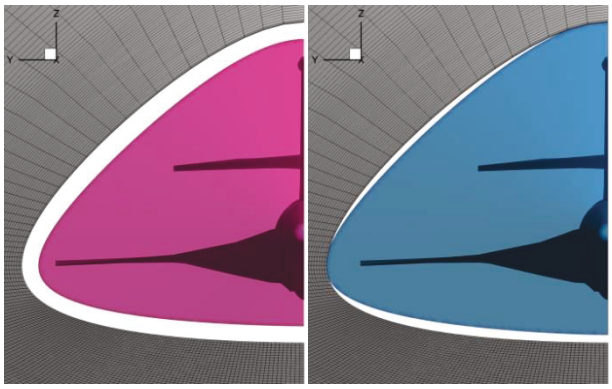

FIG 3. Modular grid interface (left side) and Chimera grid farfield (right side), both with non-cylindrical core grids

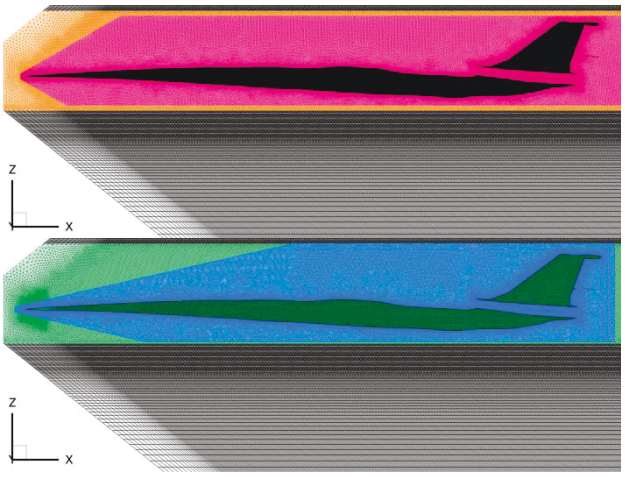

FIG 4. Modular grid symmetry plane (top) and Chimera grid symmetry planes (bottom)

The core part if filled with isotropic tetrahedral cells of constant size. Figure 3 shows the front view of the grid. For previous grid generation approaches, the core part has had a circular cross section. The best-practice developed for this paper uses a non-circular cross section of the core part. As a result, the number of unaligned tetrahedral cells below the aircraft is smaller. By that the preservation of the pressure waves can be improved. For this reason the extent of the core grid should be as small as possible. It is just slightly larger than the span of the wing, as shown in figure 3. Due to the modular grid generation approach some extra space in radial direction is needed because CENTAUR requires the cells on both sides of the interface to be tetrahedral.

In total the core grid consists of about 5 million nodes.

3.3. Collar Grid

The best-practice for grid-generation developed at DLR includes a fully structured collar grid. It extends to seven body lengths in radial direction, begins 0.1 body lengths in front of the geometry and ends at 2 body lengths aft of the geometry. Figure 4 shows the grids on the symmetry plane for the grid deformation approach and the Chimera approach. The first cell of the collar grid with respect to the core grid should be isotropic to prevent numerical errors.

In streamwise direction the grid resolution is identical with the general surface solution (433 points per body length) to ensure a crisp resolution of the shocks and expansions. In radial direction the collar grid is divided into two parts. The innermost part consists of 35 points in radial direction with a constant spacing. This ensures good quality donor cells with a constant size for the Chimera interpolation technique as well as a good cell quality after grid deformation. The outer part consists of 100 points. The cell size is growing with increasing radius by a constant stretching factor of about 1.05. In circumferential direction 96 points are evenly distributed in the bottom part of the collar grid. The flow field above the aircraft geometry is less important for the sonic boom, so the cell size is growing above the aircraft geometry. These curves in circumferential direction are discretized by 30 points.

The collar grid has to be regenerated for every Mach number since the cells should be aligned to the Mach cone. The number of points is kept constant for all cases even if the curve lengths change due to different Mach angles. In total the collar grid consists of about 9 million nodes.

4. NUMERICAL SETUP

The CFD simulations are performed with the DLR TAU code [18]. It is based on an unstructured finite-volume approach for solving the Euler or Reynolds-averaged Navier-Stokes (RANS) equations on hybrid grids. The second-order accurate AUSMDV upwind scheme is applied for the spatial discretization of the convective fluxes and an implicit lower upper symmetric Gauss Seidel scheme is used for time stepping. The gradients are computed using a Green Gauss approach. The limiting strategy by Barth and Jesperson is used to stabilize the numerical scheme. All simulations are executed without multigrid acceleration. For this study 22 inviscid simulations were conducted.

4.1. Convergence

At the first iterations of the simulation an algorithm adjusts the angle of attack to achieve the same lift as the reference configuration. For each angle of attack a Cauchy convergence criterion for the lift is used. The

termination criterion is reached if the difference to the reference lift is less than 0.5%.

The aerodynamic coefficients cannot be used as convergence criterion for the pressure signatures, because it takes a couple thousand iterations for the pressure to reach the extraction locations in the farfield, as described in detail in [12]. After the lift is converged the simulation is restarted for 7000 iterations to ensure the convergence of the pressure signatures in the farfield.

4.2. Pressure Signature Extraction

Figure 5 shows the pressure contours in the symmetry plane and the process of near-field pressure signature extraction from the three-dimensional field data along the X-coordinate. The pressure signatures are extracted at lines identified by their radius R and off-track angle Φ.

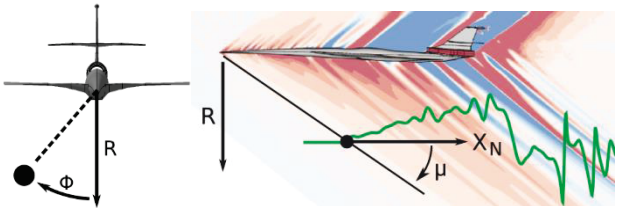

FIG 5. Pressure contour and pressure signature extraction

The distance from the nose in freestream direction X is normalized by the Mach angle μ and the body length L:

(1) $$X_N/L = (X - \frac{R}{\tan(\mu)})/L$$

Pressure amplitudes of axisymmetric wave fields decrease with the square root of distance from the aircraft [19]. In sufficient distance from the aircraft the wave field can be treated as locally axisymmetric, so the pressure signatures in this paper are normalized by the square root of R/L.

4.3. Off-Design Flight Conditions

Figure 6 gives an overview of the selected off-design flight conditions. The altitude H is changed in steps of 1000m in a range of 10,760m to 17,760m. Furthermore, the Mach number is changed in steps of M=0.1 in a range of M=1.2 to M=1.8. Additionally, a combination of lower altitude and lower flight Mach number is used. After analyzing the first Chimera results and comparing them to the grid deformation results the Chimera simulations were limited to some selected flight conditions. Beside the design point, flight condition with a separately increased and decreased flight Mach numbers and altitudes were selected.

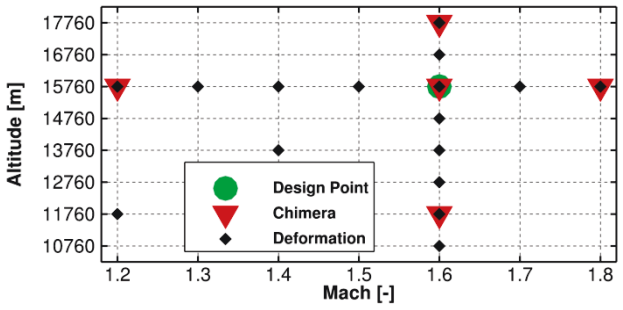

FIG 6. Overview of the selected off-design flight conditions

Table 1 shows the resulting differences in the angles of attack for the off-design flight conditions. The differences in angle of attack between simulations with the grid deformation and the Chimera technique for the same flight conditions are below 0.01°, so only one value is listed in this table.

Altitude [m]	Δα [°]	Mach [-]	Δα [°]
17,760	0.86	1.8	- 0.62
15,760	0	1.6	0
13,760	- 0.63	1.4	0.94
11,760	- 1.09	1.2	1.67

TAB 1. Angles of attack for different off-design flight conditions

5. RESULTS

This chapter describes the results of the new grid setup and the differences between grid deformation and the Chimera technique.

5.1. Validation of the Non-Circular Core Grid

For this paper the core grid layout was modified, as described in chapter 3.2. Figure 7 shows the pressure signatures for the CENTAUR-generated grid with a circular core cross section and the new grid generation approach described in this paper. The grid provided by SBPW2 is shown as a reference.

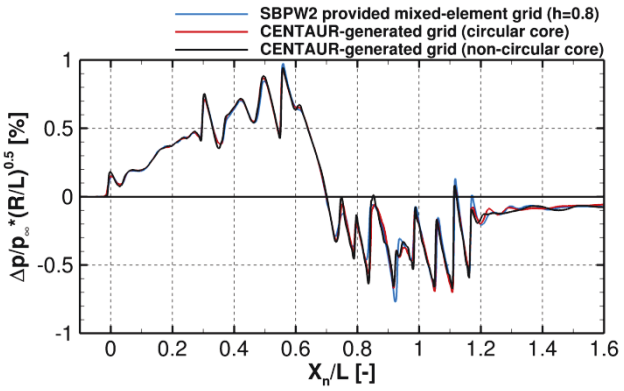

FIG 7. Pressure signatures at R/L=5 and Φ=0° for different grids

The agreement between the considered grids is very good, while the workshop-provided grid has about 52 million grid nodes, whereas the CENTAUR-generated grids only have about 15 million grid nodes. The non-circular core grid does not have a negative impact on the pressure signatures. The magnitudes of shocks and expansions are slightly better preserved. Some slight differences can be found for $0.9<X_N<1$. This is also the part in the pressure signature that was identified to be most sensitive to the grid resolution at SBPW2 [9, 12]. These differences can be traced back to reflections of the nacelle inlet shock on the upper wing and lower HTP surface. Further details for the validation of the CENTAUR-generated grid with a cylindrical core can be found in [12].

5.2. General Comparison of Grid Deformation to the Chimera Technique

Table 2 shows the comparison of grid node numbers, iterations and simulation runtimes for a selected flight condition with modified angle of attack. All simulations were run on 6 nodes (144 cores) on the C²A²S²E cluster. Even though the required iterations to converge the lift are lower when using the Chimera technique, the total number of grid nodes is higher and the Chimera interpolation process requires some additional runtime. As a result, the total simulation runtime is higher for the simulations with the Chimera technique.

	Grid Deformation	Chimera Technique
Number of grid nodes	14,282,835	15,751,782
Simulation runtime (144 cores)	1:17h	1:48h
Iterations	9,666	9,478

TAB 2. Comparison of grid node numbers and simulation runtimes for the simulations at M=1.6 at an altitude of 11,760m

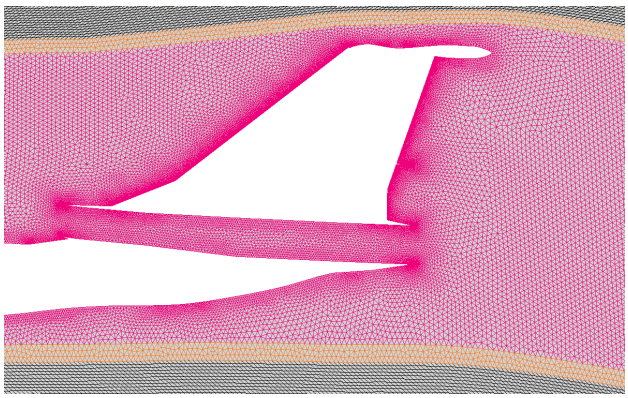

FIG 8. Deformed symmetry plane grid for H=11,760m and Δα =-1.09°

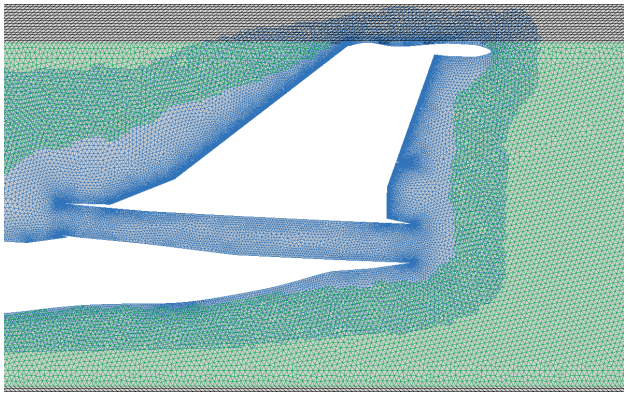

FIG 9. Chimera symmetry plane grids for H=11,760m and Δα =-1.09°

Figure 8 shows the symmetry plane of the deformed grid for an altitude of 11,760m. For this angle of attack the cells below the aircraft are slightly stretched while the cells above the aircraft are squeezed. This leads to a slight misalignment of the cells below the aircraft with regard to the Mach cone. The impact of the misalignment will be discussed in the following chapter.

Figure 9 shows the results of the automatic hole cutting algorithm for the Chimera technique at the same angle of attack. The hole cutting algorithm ensures a sufficiently large overlapping region. The cells sizes in the overlapping region are most widely identical with minor differences in the region above the VTP.

5.2.1. Pressure Signature Comparison

For an adequate comparison also the flow solutions have to be compared for the two techniques. Figure 10 shows the on-track pressure signatures at 5 body lengths distance for the grid deformation and the Chimera technique.

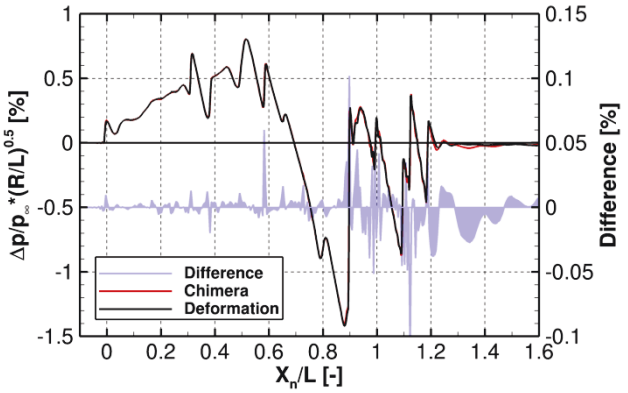

FIG 10. Pressure signatures at R/L=5 and Φ=0° for the Chimera grids and deformed grids

The agreement between both pressure signatures is very good. For a better comparison the difference between the pressure signatures is depicted on a larger scale in figure 10. Strong peaks represent differences in the positions of shocks, while differences in the pressure level appear as an area. The differences increase in streamwise direction and are strongest aft of the aircraft.
The differences decrease with increasing off-track angle, because the alignment of the cells to the Mach cone is better at high off-track angles. The differences for the other compared flight conditions are very similar to the ones shown in figure 10.

5.2.2. Flow Solution Comparison

Figure 11 shows the Mach cone aligned pressure contours on the symmetry plane at the transition from the core to the collar part of the grid. Even though the cells are aligned to the freestream Mach angle, the locally higher Mach angle leads to a slight misalignment of the cells of the Chimera grid. The misalignment of the cells of the deformed grid is even stronger and leads to a different pressure propagation. This explains the peak in the pressure signature difference at $X_N/L=0.9$.
Figure 12 shows the Mach cone aligned pressure contours on the symmetry plane in direct vicinity of the aircraft. The Chimera interpolation appears to be smooth and the shape of the pressure contours is identical to the shape of the pressure signatures for the deformed grid.

Compared to differences between different grid refinement levels [12] or even different flight conditions, the differences in the flow solutions are negligible.

This leads to the conclusion that both techniques are feasible for an accurate prediction of the sonic boom. Since the simulation runtime is lower when using the grid deformation approach, the study of the varied flight conditions is based solely on the grid deformation approach.

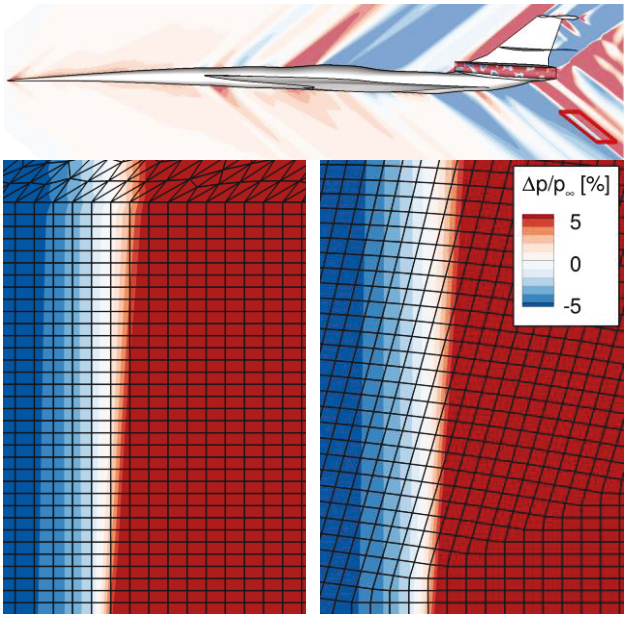

FIG 11. Mach cone normalized Chimera (left) and deformed (right) symmetry plane grids for H=11,760m and Δα=-1.09°

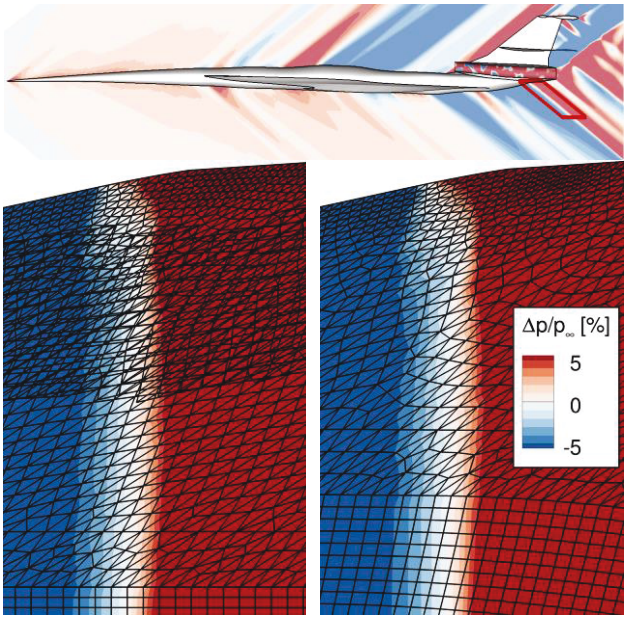

FIG 12. Mach cone normalized Chimera (left) and deformed (right) symmetry plane grids for H=11,760m and Δα=-1.09°

5.3. Off-design Pressure Signatures

After verifying the two approaches to dynamically change the angle of attack the results of the variation of the flight conditions are evaluated in this chapter.

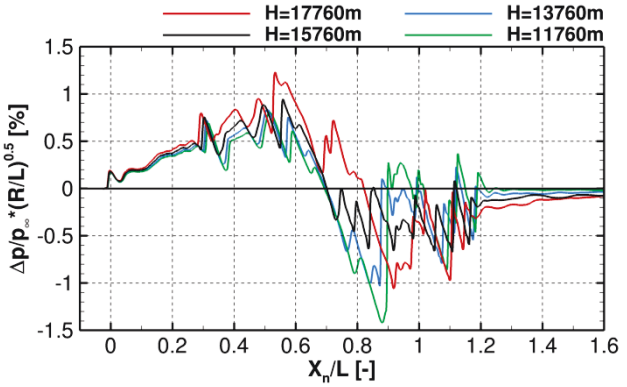

FIG 13. Pressure signatures at R/L=5 and Φ=0° for varied flight altitudes (M=1.6)

Figure 13 shows the pressure signatures for different flight altitudes. For inviscid simulations the normalized pressure difference ($\Delta p/p_\infty$) for the same angle of attack has to be identical since it is only characterized by the Mach number. As a consequence, the differences seen in Figure 13 are only a result of the different angles of attack required to achieve the same lift force. With decreasing altitude the required angle of attack decreases and thus the magnitude of the overpressure at the front part of the signature. The effect on the aft part is more complex. The most significant change is the larger magnitude of the pressure at the main expansion (X_N/L=0.9) and the recompression aft of the main expansion. As a consequence, it is very likely that the C25D will not satisfy the low boom requirements during a common segment of supersonic acceleration at a constant altitude of 11,760m. Also the fuel-efficient descend during acceleration does not seem to satisfy low-boom requirements.

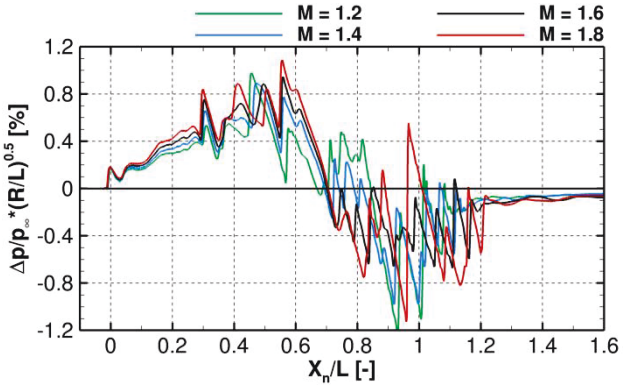

FIG 14. Pressure signatures at R/L=5 and Φ=0° for varied flight Mach numbers (H=15,760m)

Figure 14 shows the pressure signatures for different flight Mach numbers. The front part of the pressure signature is only marginally influenced since the nose is relatively axisymmetric. In this region the pressure levels increase with increased Mach numbers. The pressure oscillations in the aft part of the pressure signature, especially the main expansions and aft shock, are strongly influenced by the Mach number.

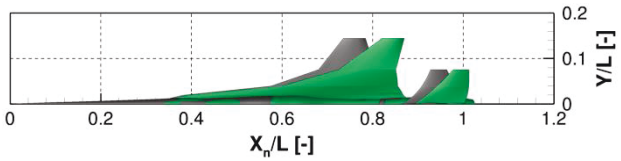

FIG 15. C25D geometry normalized by the Mach angle (grey: M=1.6, green: M=1.2)

Figure 15 shows the C25D geometry normalized by the freestream Mach angles and helps understanding the three-dimensional effects in figure 14. At $X_N/L=0.4$ the wing begins and causes interactions which depend on the Mach angle. With increasing wing span the Mach angle dependency also increases. The wing shock leads to the increased pressure level at $0.7<X_N/L<0.8$ for the simulation at M=1.2. The magnitudes of the oscillations due to the aft-wing shock and the HTP-shock are increasing when the Mach number is lowered. For M=1.2 they form two strong distinct shocks and expansions.

5.4. Off-design Pressure Contours and Possible Mission Trajectory

The comparison of the pressure signatures of different off-track angles is very complex. Instead of comparing pressure signatures, figure 16 shows the pressure contours for a quarter cylinder extracted at 5 body lengths distance. The Y axis represents the off-track angle. The contour colors represent the difference between the solution at H=15,760m and H=11,760m. The difference seen in the main expansion at $X_N/L=0.9$ in figure 13 can also be seen in this figure. Additionally, a crescentic shaped area of difference can be seen in front of $X_N/L=0.8$ due to the wing shock, which cannot be found in the on-track pressure signature.

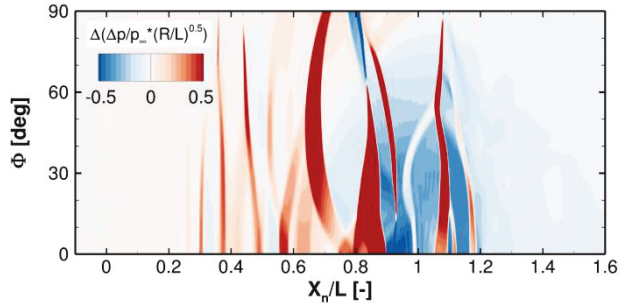

FIG 16. Cylinder extraction at R/L=5; Difference between H=15,760m and H=11,760m

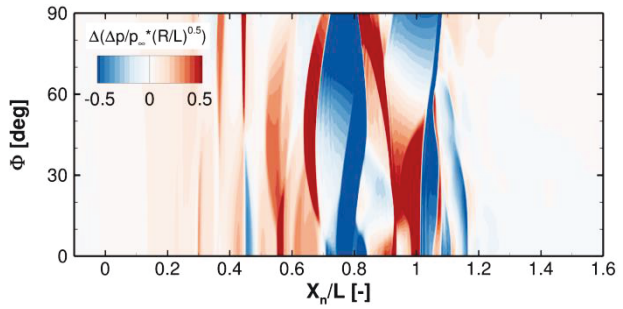

FIG 17. Cylinder extraction at R/L=5; Difference between M=1.6 and M=1.2

Figure 17 shows a similar difference contour plot for the difference between the design Mach number of M=1.6 and a lower Mach number of M=1.2. The crescentic shaped area in front of $X_N/L=0.8$ can also be seen in this plot.

By overlaying these figures it can be noticed that the effect of a lower flight altitude and a lower Mach number appears conversely in some areas, especially around $X_N/L=0.8$ and $X_N/L=1.0$.

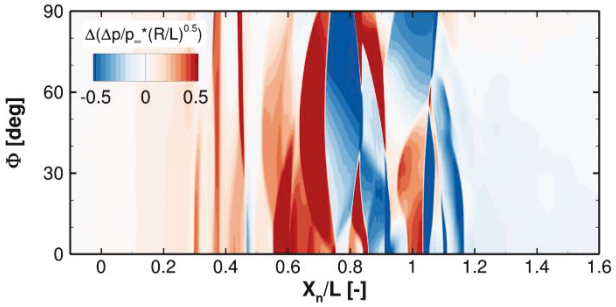

FIG 18. Cylinder extraction at R/L=5; Difference between H=15,760m, M=1.6 and H=11,760m, M=1.2

Figure 18 shows the contours for the difference in pressure between cruise flight conditions (H=15,760m, M=1.6) and a low altitude, low Mach simulation (H=11,760m, M=1.2). The strong pressure differences at $X_N/L=0.8$ and $X_N/L=1.0$ could be lowered for the on-track angle as expected. Besides the on-track angle the differences in this plot seem quite high, so the pressure signatures for these cases have to be evaluated. Additionally, a case with a flight Mach number of 1.4 at an altitude of 13,760m is regarded.

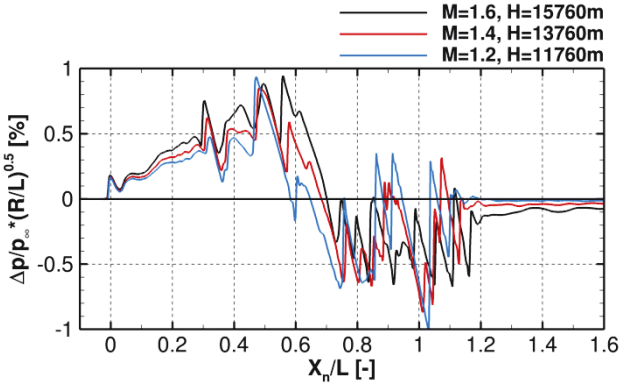

FIG 19. On-Track pressure signatures if both, flight Mach number and altitude are lowered (R/L=5 and Φ=20°)

Figure 19 shows the pressure signatures for the cases mentioned. Although the pressure oscillations in the aft part of the signature are increasing in strength compared to the designed flight conditions, the peaks are lower than it was observed for the cases at constant altitude or constant Mach number. Especially the shock at $X_N/L=0.9$ and the expansion at $X_N/L=1.0$ might still be too strong to fullfill low boom requirements under these flight conditions.

Figure 20 and 21 show the pressure signatures for these flight conditions for off-track angles of 20° and 50°. These pressure signatures are characterized by the wing shock and expansion. At the off-track angles the shock and expansion pattern is less influenced compared to the

on-track angle. Mainly the magnitudes of the shocks and expansions are changing. With decreasing Mach numbers and altitudes the magnitudes of the pressure oscillations decrease.

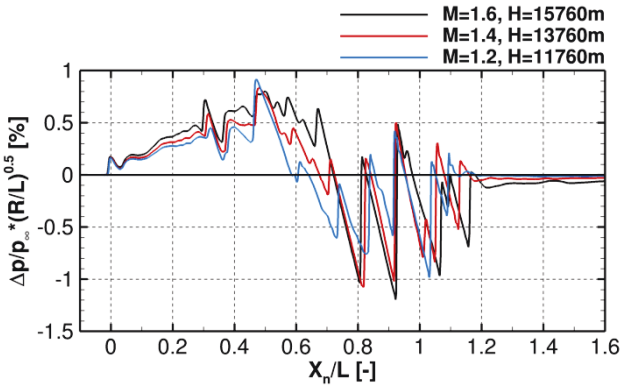

FIG 20. Off-Track pressure signatures if both, flight Mach number and altitude are lowered (R/L=5 and Φ=20°)

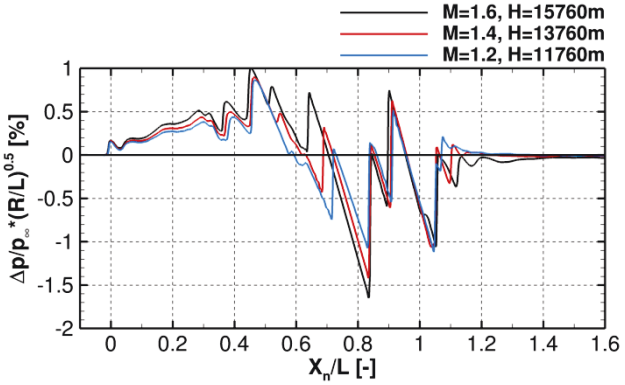

FIG 21. Off-Track Pressure signatures if both, flight Mach number and altitude are lowered (R/L=5 and Φ=50°)

A lower flight Mach number requires a lower angle of attack, whereas a lower flight altitude requires a higher angle of attack. When combining both, the resulting angle of attack is quite similar to the cruise angle of attack. The needed change in angle of attack for H=11,760m and M=1.2 is only 0.37° compared to the design angle of attack. For H=13,760m and M=1.4 the change in angle of attack is only 0.16°.

5.5. Forces and Moments

The influence of the flight altitude on lift, drag and the pitching moment is shown in figure 22. Reference for the relative forces and moments is the cruise flight condition. Only Euler computations were conducted, so no viscous effects are included in the forces and moments. The pitching moment is measured relative to the nose. According to the convergence criteria for the target lift, the lift changes are less than 0.5% for all cases. Due to the increasing density at lower altitudes the pressure drag increases by up to 80%. The pitching moment decreases by about 5%.
Figure 23 shows the influence of the flight Mach number on lift, drag and the pitching moment. It can be observed that the design of the C25D is optimized for Mach numbers around M=1.4 and M=1.6 since the drag at these speeds is lowest.

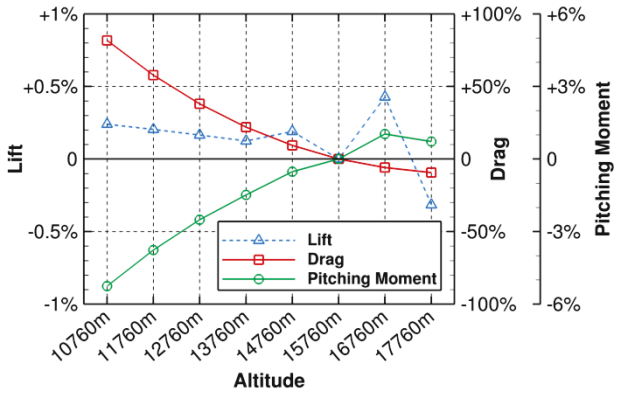

FIG 22. Influence of the flight altitude on lift, drag and the pitching moment (M=1.6)

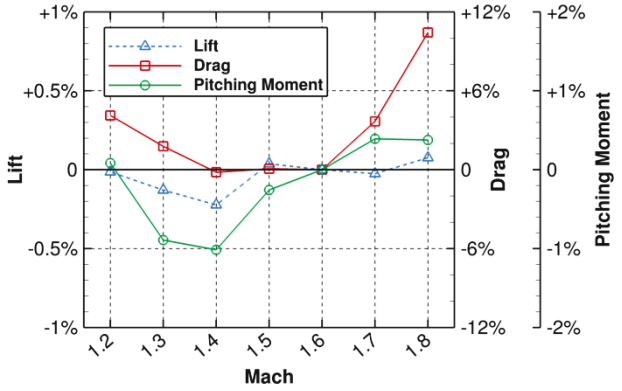

FIG 23. Influence of the flight Mach number on lift, drag and the pitching moment (H=15,760m)

6. SUMMARY

In this paper, the C25D low-boom geometry from the Second AIAA Sonic Boom Prediction Workshop was used to conduct numerical simulations at off-design flight conditions with the DLR TAU code. The flight altitude and flight Mach number were varied to simulate different flight conditions of a possible mission trajectory while the lift was kept constant.

Keeping the lift constant requires the angle of attack to be adapted, which is not straight forward possible with the Mach cone aligned farfield used for sonic boom simulations. The focus of this paper is the assessment of a new approach for grid generation with a non-circular core grid as well as the evaluation of the grid deformation and Chimera technique to change the angle of attack. Both techniques are viable for the variation of the angle of attack for low boom simulations. The differences in the pressure fields of simulations with the two techniques are negligible for all flight conditions. The grid deformation technique was preferred for the simulations because of lower simulation runtimes.

In total, 22 different simulations were conducted with different flight altitudes and flight Mach numbers to gain an understanding of the occurring effects when changing the flight conditions. Both parameters have strong impact on the pressure signatures, especially in the aft part of the signature. The interaction of the shocks and expansions is

changed and they are not merging for off-design flight conditions.

As a consequence, it seems very likely that the C25D will not satisfy low boom requirements during a common segment of supersonic acceleration at a constant altitude of 11,760m and the mission trajectory or design has to be modified to fullfill the low boom requirements.

7. OUTLOOK

The near-field results considered in this paper do not allow a quantitative assessment of the perceived ground loudness. By evaluating the near-field pressure signatures of the C25D the author assumes that a continuous climb during acceleration might lead to the lowest sonic boom. Since even small differences in the pressure signatures can have a large impact on the perceived loudness level, upcoming studies will have to include a ground propagation algorithm and an exposed sound level measure to evaluate this assumption.

After the implementation of a ground propagation algorithm and a loudness measurement algorithm, DLR intends to design and optimize a supersonic civil aircraft toward low boom – low drag. For this purpose the grid deformation technique verified in this paper is of great importance. The optimization should also incorporate a possibility to trim the aircraft, since trim might have an influence on the low boom characteristics.

Furthermore, two very important aspects for the development of a low boom aircraft are the computation of the focus of the sonic boom while accelerating and understanding the community response to the sonic boom.

8. ACKNOWLEDGMENTS

The author would like to thank the creators of the C25D model geometry and the SBPW2 organizing committee for making a low boom geometry publically available which can be used for further studies.

9. REFERENCES

[1] B. Liebhardt and K. Lütjens: “An Analysis of the Market Environment for Supersonic Business Jets”, 60. Deutscher Luft- und Raumfahrtkongress - Manuskripte, 2011, pp. 617-627, DLRK 241457

[2] B. Liebhardt, K. Lütjens and V. Gollnick: “Estimation of the Market Potential for Supersonic Airliners via Analysis of the Global Premium Ticket Market”, 11th AIAA Aviation Technology, Integration, and Operations Conference, 2011, AIAA Paper 2011-6806

[3] I. Ordaz, K. A. Geiselhart, J. W. Fenbert: „Conceptual Design of Low-Boom Aircraft with Flight Trim Requirement”, Journal of Aircraft, Vol. 52, No. 3, 2015, pp. 932-939

[4] Spike Aerospace, Inc: “Spike S-512 Specifications & Performance” [online web site], URL: http://www.spikeaerospace.com, [accessed 28th August 2017]

[5] B. Liebhardt, F. Linke and K. Dahlmann: “Supersonic Deviations: Assessment of Sonic-Boom-Restricted Flight Routing”, Journal of Aircraft, Vol. 51, No. 6, 2014, pp. 1987-1996

[6] Boom Technology, Inc [online web site], URL: https://boomsupersonic.com, [accessed 28th August 2017]

[7] Aerion Corporation: “Aerion AS2” [online web site], URL: http://www.aerionsupersonic.com/, [accessed 28th August 2017]

[8] R. Seebass and B. Argrow: “Sonic Boom Minimization Revisited”, 2nd AIAA Theoretical Fluid Mechanics Meeting, 1998, AIAA Paper 1998-2956

[9] M. A. Park and M. Nemec: “Near Field Summary and Statistical Analysis of the Second AIAA Sonic Boom Prediction Workshop”, 35th AIAA Applied Aerodynamics Conference, 2017, AIAA Paper 2017-3256

[10] I. Ordaz, M. Wintzer and S. K. Rallabhandi: “Full-Carpet Design of a Low-Boom Demonstrator”, 33rd AIAA Applied Aerodynamics Conference, 2015, AIAA Paper 2015-2261

[11] J. Kirz and R. Rudnik: “DLR Simulations of the First AIAA Sonic Boom Prediction Workshop Cases”, 55th AIAA Aerospace Sciences Meeting, 2017, AIAA Paper 2017-0276

[12] J. Kirz and R. Rudnik: “DLR TAU Simulations for the Second AIAA Sonic Boom Prediction Workshop”, 35th AIAA Applied Aerodynamics Conference, 2017, AIAA Paper 2017-3253

[13] H. Suzuki: “Trajectory Design of Silent Supersonic Technology Demonstrator (S3TD)”, 26th Congress of the International Council of the Aeronautical Sciences, 2008, ICAS Paper 2008-5.7.5

[14] M. A. Park, R. L. Campbell, A. Elmiligui, A., S. E. Cliff and S. N. Nayani: “Specialized CFD Grid Generation Methods for Near-Field Sonic Boom Prediction”, 52nd Aerospace Sciences Meeting, 2014, AIAA Paper 2014-0115

[15] CentaurSoft: “CENTAUR - Mesh (Grid) Generation for CFD and Computational Simulations”, [online web site], URL: http://www.centaursoft.com, [accessed 28th August 2017]

[16] J. L. Steger, F.C. Dougherty and J. A. Benek: “A Chimera Grid Scheme”, Advances in Grid Generation, edited by K.N. Ghia and U. Chia, ASME FED-5, 1983, pp 59-69

[17] A. de Boer and M. S. van der Schoot and H. Bijl: “Mesh deformation based on radial basis function interpolation”, Computers & Structures. Vol. 85, 2007, pp. 784–795

[18] D. Schwamborn, T. Gerhold and R. Heinrich: “The DLR TAU-Code: Recent Applications in Research and Industry”, European Conference on Computational Fluid Dynamics ECCOMAS CFD, 2006

[19] K. Plotkin: “Review of Sonic Boom Theory”, 12th Aeroacoustics Conference, 1989, AIAA Paper 1989-1105